Potassium pre-inserted $K_{1.04}Mn_8O_{16}$ cathode materials for aqueous Li-ion and Na-ion hybrid capacitors

Yamin Zhang[a,c] , Lina Chen[a,b] ,Chongyang Hao[a], Xiaowen Zheng[a], Yixuan Guo[b], Long Chen[a], Kangrong Lai*[c], Yinghe Zhang*[d], Lijie Ci*[a,b]

[a]SDU & Rice Joint Center for Carbon Nanomaterials, Key Laboratory for Liquid-Solid Structural Evolution & Processing of Materials (Ministry of Education), School of Materials Science and Engineering, Shandong University, Jinan 250061, China

[b] School of Materials Science and Engineering, Harbin Institute of Technology, Shenzhen 518055, China

[c] Department of Physics, Changji University, Changji 831100, China

[d] LEO group CO., Ltd., Block A, Yuanzhong Building, No. 2900, Zhongshan North Road, Shanghai, China

Abstract

For the applications of aqueous Li-ion hybrid capacitors and Na-ion hybrid capacitors, potassium ions are pre-inserted into MnO_2 tunnel structure, the as-prepared $K_{1.04}Mn_8O_{16}$ materials consist of nanoparticles and nanorods were prepared by facile high-temperature solid-state reaction. The as-prepared materials were well studied andthey show outstanding electrochemical behavior. We assembled hybrid supercapacitors with commercial activated carbon (YEC-8A) as anode and $K_{1.04}Mn_8O_{16}$ as cathode. It has high energy densities and power densities. Li-ion capacitors reach a high energy density of 127.61 Wh kg^{-1} at the power density of 99.86 W kg^{-1} and Na-ion capacitor obtains 170.96 Wh kg^{-1} at 133.79 W kg^{-1}. In addition, the hybrid supercapacitors demonstrate excellent cycling performance which maintain 97 % capacitance retention for Li-ion capacitor and 85 % for Na-ion capacitor after 10,000 cycles.

1. Introduction

With deteriorating of environment and consuming of resouse, There is a growing need for portable, environmentally friendly new energy storage devices [1-3]. Lithium-ion batteries dominate the market owing to their high energy densities, but they suffer low power density attribute to the polarization occurs at high charge and discharge rates, and poor cycle life due to the degradation of the structure during lithium ion intercalation/deintercalation[4-5]. Supercapacitors are excellent energy storage systems, which can store and transmit energy at much higher rate compared with batteries, because the reaction mechanism of energy storage is a simple charge separation process at the interface of electrode and electrolyte[6-8]. Hence, they deliver high power density and long cycle life. But they have comparatively low energy density because the adsorption/desorption just take place at surface of active materials. Hybrid supercapacitor (HSC), combining battery electrode and capacitor electrode, have both the advantages of batteries and tsupercapacitors. It has a higher energy density than supercapacitor, and at the same time retain cycling stability. However, the slow charging and discharging rate of battery-type materials limits its power density, which makes the hybrid device unable to be charge-discharged as fast as double-layer electric capacitors. Therefore, it's of great importance to enhance the rate performance of battery-type materials[9].

Nanocrystallization is an effective way to improve the utilization and performance of active materials[10-12]. The smaller the crystal size, the larger the specific surface area, the electrode material and electrolyte can better contact, which

its specific capacity, shorten the diffusion distance of ion, improve the electrochemical reaction rate[13]. Manganese-based materials have been widespread used as positive electrode material because of its abundant reserves, low cost ,low toxicity and high theoretical capacity [14-17]. Manganese dioxide (MnO_2) is commonly used as electrode materials for supercapacitors due to its low cost, easy preparation and good electrochemical properties[18-21]. In recent years, there have been a large number of reports about manganese-based materials using different ways to synthesize nanoparticles, nanowires, nanorod, ultrathin nanocrystals and so on[10, 12, 14, 22-23]. However, MnO_2 still suffer(s) from sluggish ion diffusion kinetics, low conductivity and volume expansion, which limits its development[24].

In order to improve the ion diffusion kinetics and inhibit volume expansion during charging and discharging process of manganese oxide materials, cations pre-embedded into nanostructures were used to control the intercrystal spacing[25-27].

Herein, we report a pre-inserted potassium ions with large ion radius to expand the spacing between crystal planes, so that lithium ions can be inserted and disinserted quickly and allows sodium ions with large ion radius inserted and disinserted freely[28]. Nanostructured $K_{1.04}Mn_8O_{16}$ (KMO) materials are prepared by facile high temperature calcination process, and the calcination process is illustrated in Fig.1 b. MnO_2 and KCO_3 are fully ground using anhydrous ethanol to get a mixture , then it is kept at 500 ℃ for 8h in air atmosphere. It can be seen that the material we obtained is composed of nanoparticles and nanorods by scanning electron microscope and high transmission power, providing it a high specific surface area. Electrochemical

properties in Li_2SO_4 and Na_2SO_4 electrolyte were studied.

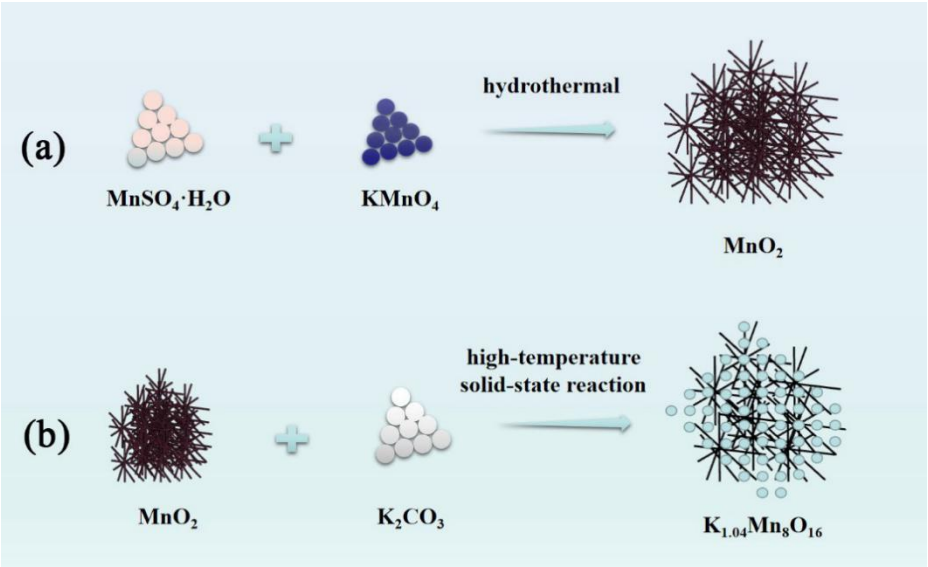

Fig.1. Schematic diagram of the preparation process of MnO_2 (a) and KMO (b).

1. Experimental

1.1 Materials are prepared

All the starting reagents ($KMnO_4$、$MnSO_4·H_2O$、K_2CO_3) were purchased from Sinopharm Chemical Reagent Co., Ltd., China, which are analytical pure.

We prepared the precursor MnO_2 by the method mentioned in our previous work[29]. Take a certain amount MnO_2 precursor and K_2CO_3 mixtured with the help of ethyl alcohol in agate mortar grind, and then transfer into annealing furnace at 500 °C for 8 h in air atmosphere with a heating rate of 5 °C/min, collect the solid product and grind.

2.2 Material characterization

The phase structure of KMO were represented by X-ray diffraction (XRD) with Rigaku MiniFlex X-ray diffractometer with Cu Ka radiation. Raman spectra were recorded by Renishaw InVia Reflex Raman spectroscope. The morphology and

elements distribution were researched by SU-70 field emission scanning electron microscope (FESEM) together with energy dispersive spectrometry (EDS). The high-resolution transmission electron microscope (HRTEM) images and selected area electron diffraction(SAED) were studied by JEM-2100 equipment at an acceleration voltage of 200 kV. X-ray photoelectron spectroscopy (XPS) was executed for valence state of material. K content in KMO materials was detected by an Optima 8000 inductively coupled plasma optical emission spectroscopy (ICP-OES) instrument.

2.3 Electrochemical performance

The preparation of electrode for electrochemical testing, active materials (85 wt%), acetylene carbon black (10 wt%) and polytetrafluoroethylene (PTFE) (5 wt%) were completely mixed in N-Methylpyrrolidone (NMP) solution to create a uniform slurry. Simultaneously, for the negative electrodes, active carbon (80 wt%), acetylene carbon black (10 wt%) and PTFE (10 wt%) were mixed in NMP solution. Spread the slurry evenly over the nickel foam with the size of 1cm×1cm, and as current collectors. The collectors were dried in a vacuum oven at 100 ℃ for 10 h. A representative three-electrode system was made up of a working electrode, the platinum sheet (1cm×1cm) and a saturated calomel reference electrode. The electrolyte here was 1M Na_2SO_4 and 1M Li_2SO_4. The Cycle voltammetry (CV), Galvanostatic charge/discharge (GCD) and electrochenical impedance spectra (EIS) were tested via a electrochemical workstation (CHI 660A). Unsymmetrical hybrid full cell capacitors were tested via a two electrode system, the full cell with a cathode and

an anode were incorporated by a membrane(Whatman) in the 1M Na_2SO_4 /1M Li_2SO_4.

The following formula can be applied to compute specific capacitance[30]:

$$C = \frac{1}{mv}\int \frac{I}{\Delta V} dV \quad (1)$$

Where m expressed total mass of active material(g), v expressed the scan rate(V s^{-1}), ΔV expressed the potential window, I expressed the response current(A) and C expressed the specific capacitance (F g^{-1}).

KMO and activated carbon(YEC-8A) were assembled into coin cells (CR2032) as cathode and anode, respectively. Before installing the coin battery, the electrode and membrane are soaked in electrolyte for 10 h to permeate the active substance.

The charge quantity satisfies this formula: q=C×V×m. To meet the relationship of $q^+=q^-$, the mass ratio of the two electrodes can be expressed via the following equation[31] :

$$\frac{M_+}{M_-} = \frac{C_- \times V_-}{C_+ \times V_-} \quad (2)$$

The subscripts "+" is cathode and "-" is the anode, C expressed the specific capacitance, V expressed the potential window and M expressed the mass.

The energy density(E) and power density(P) are calculated on the basis of the following equations[32]:

$$E = \frac{1}{7.2} CV^2 \quad (3)$$

$$P = \frac{3600 \times E}{\Delta t} \tag{4}$$

Where Δ t expressed the discharging time (s).

3 Results and discussion

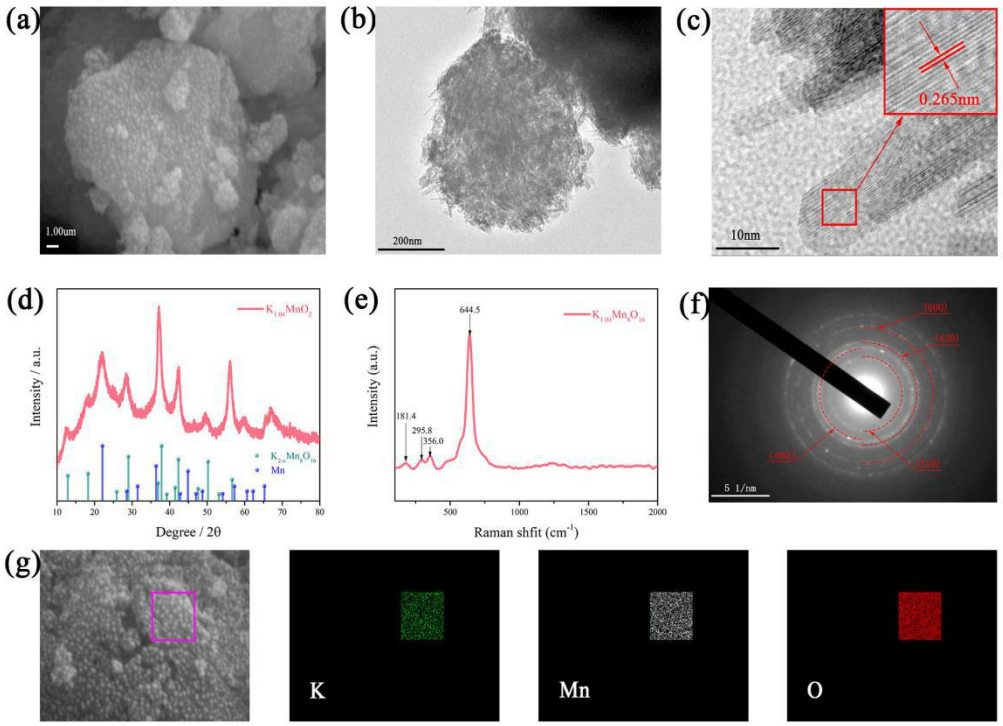

Figure.2. Characterization of KMO: (a) SEM image. (b) TEM image and (c) HRTEM image. (d) XRD pattern and (e) Raman pattern. (f) SAED pattern. (g) SEM image and conform corresponding elemental mapping of K, Mn and O.

3.1 structural characterization

The KMO prepared through high-temperature calcination process is illustrated in Fig.1. MnO_2 and K_2CO_3 are fully ground with the help of anhydrous ethanol, then keep this mixture at 500 ℃ for 8h n air atmosphere. The XRD pattern of KMO is shown in fig. 2d, whose the characteristic packs conform to the reference values of

$K_{2-x}Mn_8O_{16}$ (PDF#42-1348). The characteristic pack at 2θ = 22° arises corresponding to the (111) crystal plane of Mn. The Selected area electron diffraction (SAED) pattern(Fig.2f), the rings are connected with (310), (400), (420), (600) crystal faces of KMO. It is consistent with the XRD results. The K content of prepared KMO was determined by ICP-OES as shown in table 1, the atomic ratio of potassium to manganese was 0.13:1. Raman pattern of KMO (Fig.2e) shows three bands situated at 181.4, 295.8 and 356.0 and 644.5 cm^{-1}. The first two peaks are assigned to the frame vibration of MnO_2. The last is assigned to the Mn-O stretching vibration of manganese oxide octahedral[33].

Table.1 ICP results of $Li_{1.04}Mn_8O_{16}$ nano-structure

Sample	K content / mg kg^{-1}	Mn content / mg kg^{-1}
$Li_{1.04}Mn_8O_{16}$	8.6	90

The electron microscope (SEM) and high resolution transmission electron microscope (HRTEM) were tested to study the as-prepared nanostructured KMO. The SEM image is displayed in Fig.2a. KMO materials are consist the nanoparticles and nanorods, on the surface is nanoparticles and the inside can be seen from TEM (Fig 2b) that nanorods are clustered together. The nanoparticles structure can greatly increase the internal area to make sure that the electrolyte is in full contact with the active material, and the nanorods furnish short ion diffusion pathways during the charging/discharging process. The Fig.2c shows the lattice fringe spacing of KMO nanorods is 0.265 nm, which in accord with the (400) crystal faces of $K_{2-x}Mn_8O_{16}$.

The EDS image of KMO is shown in Fig.2g, element mapping of potassium, manganese, oxygen are uniformly distributed, which further proves the potassium element existence in the obtained KMO together with manganese and oxygen.

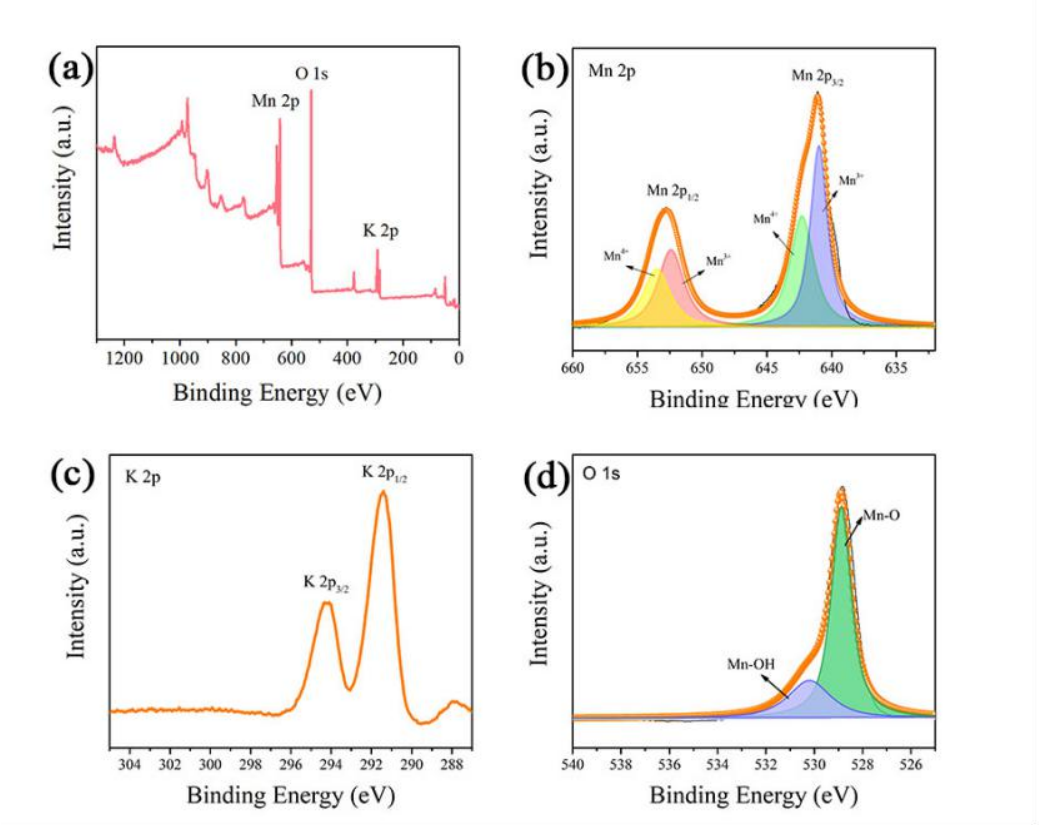

Fig. 3. XPS spectrum analysis of the KMO ： (a) XPS survey. (b) K 2p, (c) Mn 2p and (d) O 1s are High-resolution spectrum.

XPS analysis was used to test the surface chemical components and correlative valent state of KMO. The Fig. 3a shows only K, Mn and O elements of XPS survey spectrum. It is correspond to the EDS results. The High-resolution Mn 2p spectrum in Fig. 3b shown two peaks situate at about 641.1 and 652.8 eV , which are allocated to Mn $2p_{3/2}$ and Mn $2p_{1/2}$ respectively[34]. The K 2p spectrum typically shows two strong XPS peaks on behalf of K $2p_{1/2}$ and K $2p_{3/2}$ in Fig. 3c [35]. The O 1s spectrum in Fig. 3d was divided into two oxygen contributions, one peak at 528.8 eV, which is relative to

the Mn-O bond, indicate that O atoms are mainly bonded with Mn. The other one peak at 530.2 eV is in connection with Mn-OH. As a consequence, according to the above results, micro-sized KMO particles consist with nanoparticles and nanorods can be successfully achieved through facile high-temperature calcination[36].

3.2 Electrochemical performance test

3.2.1 For Li-ion hybrid capacitors

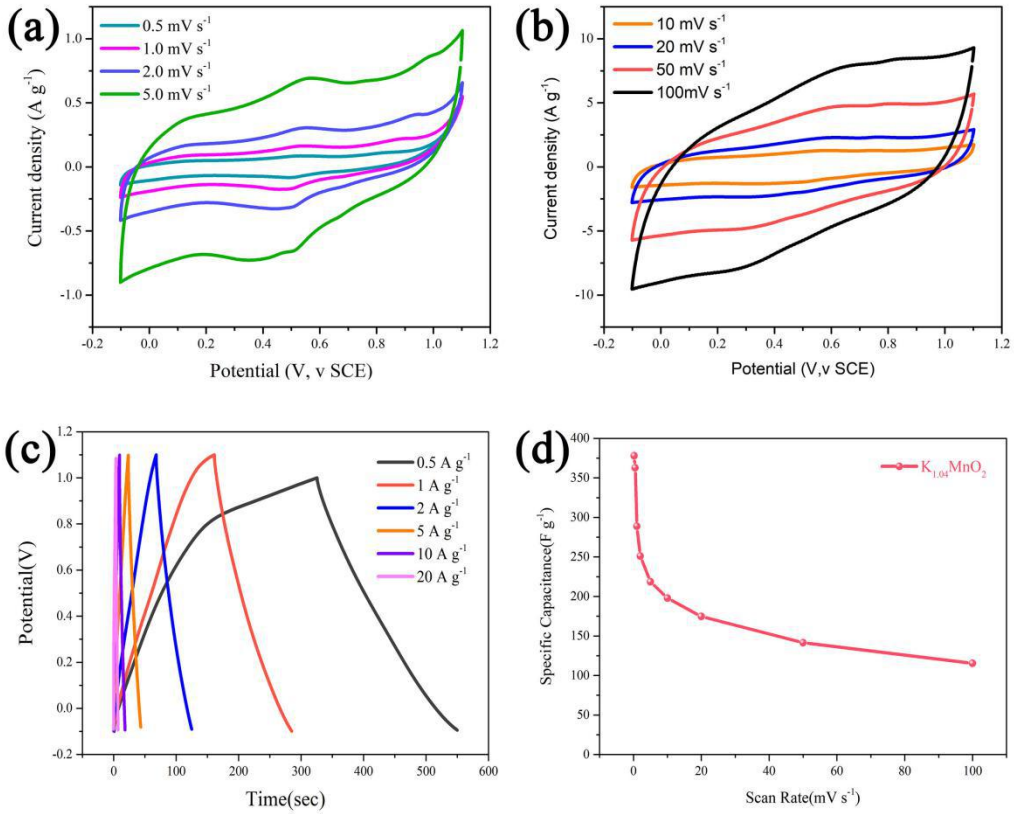

Fig. 4. Electrochemical performance of the KMO electrodes in Li_2SO_4 aqueous electrolyte: (a) and (b) CV curves at different scan rates. (c) The typical charge-discharge profiles at different various current densities. (d) Specific capacitance of KMO at different scan rates.

The electrochemical properties of KMO materials were evaluated with 1M Li_2SO_4 aqueous electrolyte in a three-electrode system. Fig. 4a shown the Cyclic

voltammetry (CV) at scan rates from 0.5 to 10 mV s^{-1} and Fig. 3b is from 20 to 100 mV s^{-1} . CV curves of KMO at different scan rates display a pair of redox peaks, which are corresponding to Li-ion deintercalation/intercaiation process, hinting the Faradic pseudocapacitive nature of KMO material. CV curves show good symmetry, and the shape of the curve does not change significantly when the sweep speed increases, indicating that it has good rate performance. The curve of constant current charge and discharge is shown in Fig. 4c, it can be seen that the charge and discharge curves are symmetrical, indicating that the material has good reversibility. Obtain high specific capacitance 362.79 F g^{-1} at a low scan rate of 0.5 mV s^{-1}, and When the high scanning rate increases to 100mv s^{-1}, a higher specific capacitance of 115.39 F g^{-1} can still be obtained. So that shows excellent electrochemical performance.

In order to match with KMO electrode and assemble a hybrid supercapacitor, activated carbon YEC-8A(YEC) was selected as the negative electrode material of hybrid supercapacitor. Electrochemical properties of YEC were tested in Li_2SO_4 aqueous electrolyte and shown in Fig. S1. CV curves are approximately rectangular at different scan rates from 0.5 to 200 mV s^{-1}, and the constant charge and discharge curves are symmetrical, indication excellent rate performance. The specific capacitance was up to 122.39 F g^{-1} at 0.5 mV s^{-1}, which makes activated carbon an ideal negative electrode material for hybrid supercapacitors. The mass ratio of KMO cathode and YEC anode is calculated to be 3:5. The CV curves at different voltage windows of KMO//YEC hybrid device is shown in Fig. 5a. it can be seen that even when the voltage window increases to 2.4V, the hybrid overcharge remains stable.

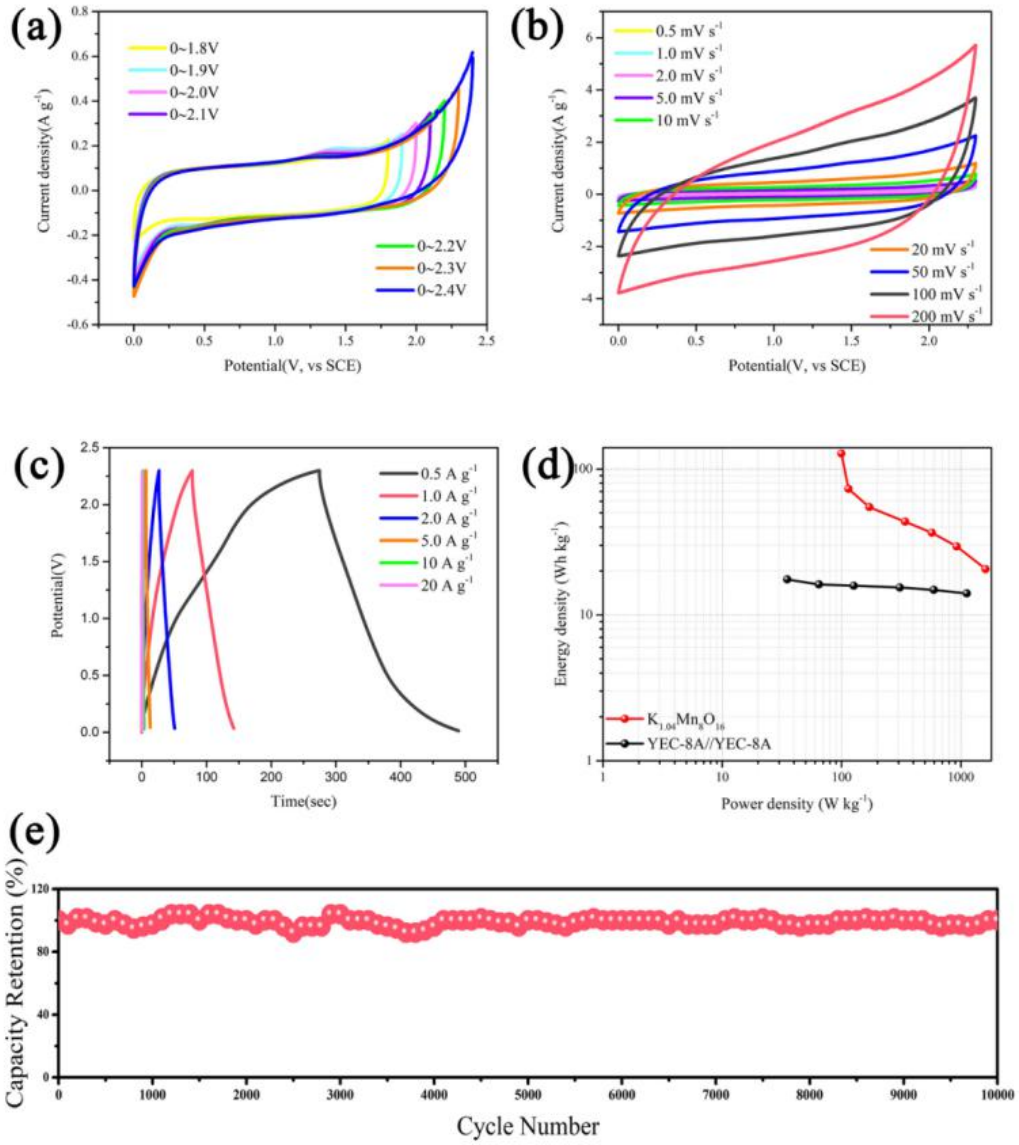

Fig. 5. Electrochemical performance of the KMO//YEC electrodes in Li-ion hybrid capacitors:(a) CV curves at different voltage windows. (b) CV curves at different scan rates. (c) The typical charge-discharge profiles at different various current densities. (d) Ragone plots . (e) Long cycle performance.

The CV (Fig. 5b)curves of KMO//YEC at different scan rates from 0.5 to 200 mV s^{-1}. The curve maintains symmetry even at high sweeping speed and shows good reversibility. The charge/discharge profiles at various densities from 0.5 to 20 A g^{-1} is shown in Fig. 5c, which symmetrical charge and discharge curves show the storage

reversibility of Li-ion hybrid capacitors.

The Ragone plot of power densities and energy densities is shown in Fig. 5d. It has a high energy density of 127.61 Wh kg^{-1} at the power density of 99.86 W kg^{-1}, and high power density of 2.3 kW kg^{-1} at the energy density of 14.5 Wh kg^{-1}， which are higher than activated carbon YEC symmetrical capacitor and some other reports shown in Table 2. The cycle performance of KMO at a current density of 1 A g^{-1} is shown in Fig. 5e.the capacitance retention reach up to 97% over 10000 cycles.

Table 2. Comparison of power density and energy density of Li-ion hybrid supercapacitors(LIHS).

Hybrid	Technology	Energy (Wh kg^{-1})	Power (W kg^{-1})	Ref.
KMO//YEC	LIHS	127.61	99.86	This work in Li_2SO_4
AC//LTO	LIHS	140.96	40.12	[37]
AC//LFP	LIHS	35	105	[38]
LFP@C//ARGOALIC	LIHS	11.5	100	[39]

3.2.2 For Na-ion hybrid capacitors

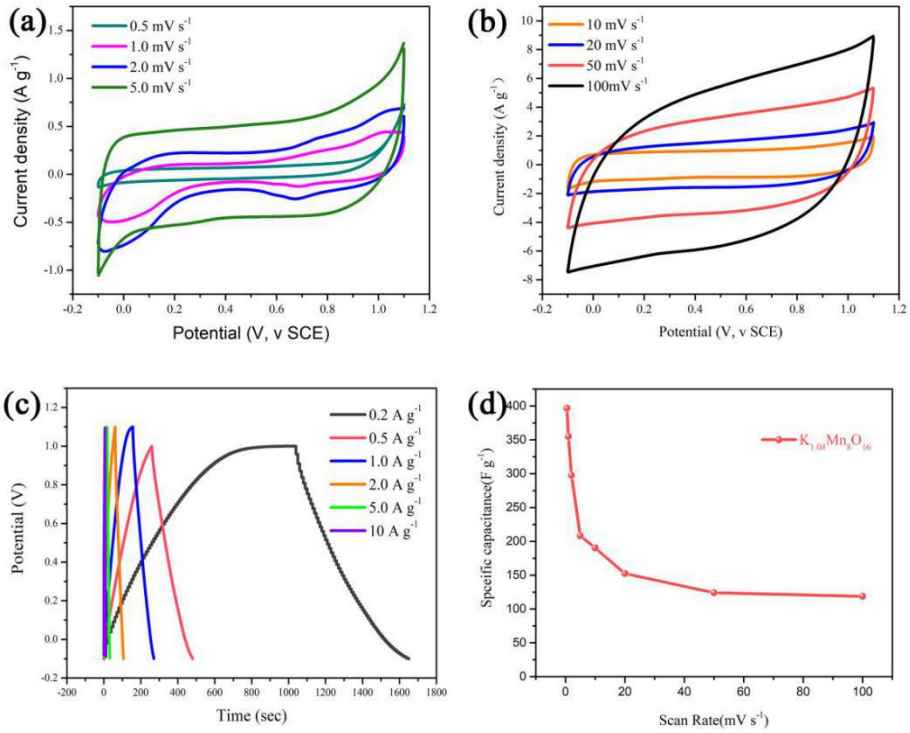

Fig. 6. Electrochemical performance of the KMO electrodes in Na_2SO_4 aqueous electrolyte: (a) and (b) CV curves at different scan rates. (c) The typical charge-discharge profiles at different various current densities. (d) Specific capacitance of KMO at different scan rates.

For the application in Na-ion capacitors, the electrochemical properties of KMO nanowires were evaluated with 1M Na_2SO_4 aqueous electrolyte in a three-electrode system. Fig. 6a shows the cyclic voltammetry (CV) at scan rates from 0.5 to 10 mV s^{-1} and Fig. 6b from 20 to 100 mV s^{-1} .The CV curves of KMO at scan rates from 0.5 to 2 mV s^{-1} display a pair of redox peaks, which are corresponding to Na-ion deintercalation/intercaiation, hinting the Faradic pseudocapacitive nature of KMO material. However, the redox peaks disappears at higher sweep rates, this may due to the large radius of sodium ion, which has no time to insert into the electrode material at higher scan rates, but only adsorb and desorb on the surface. The curves of constant current charge and discharge are shown in Fig. 6c, it can be seen that the charge and

discharge curves are symmetrical, indicating good reversibility. The Specific capacitance of KMO (Fig.4d) shows a high specific capacitance of 396.73 F g^{-1} at a low scan rate of 0.5 mV s^{-1}. when the scan rate increases to 100 mV s^{-1}, still can be obtained specific capacitance of 102.78 F g^{-1}.

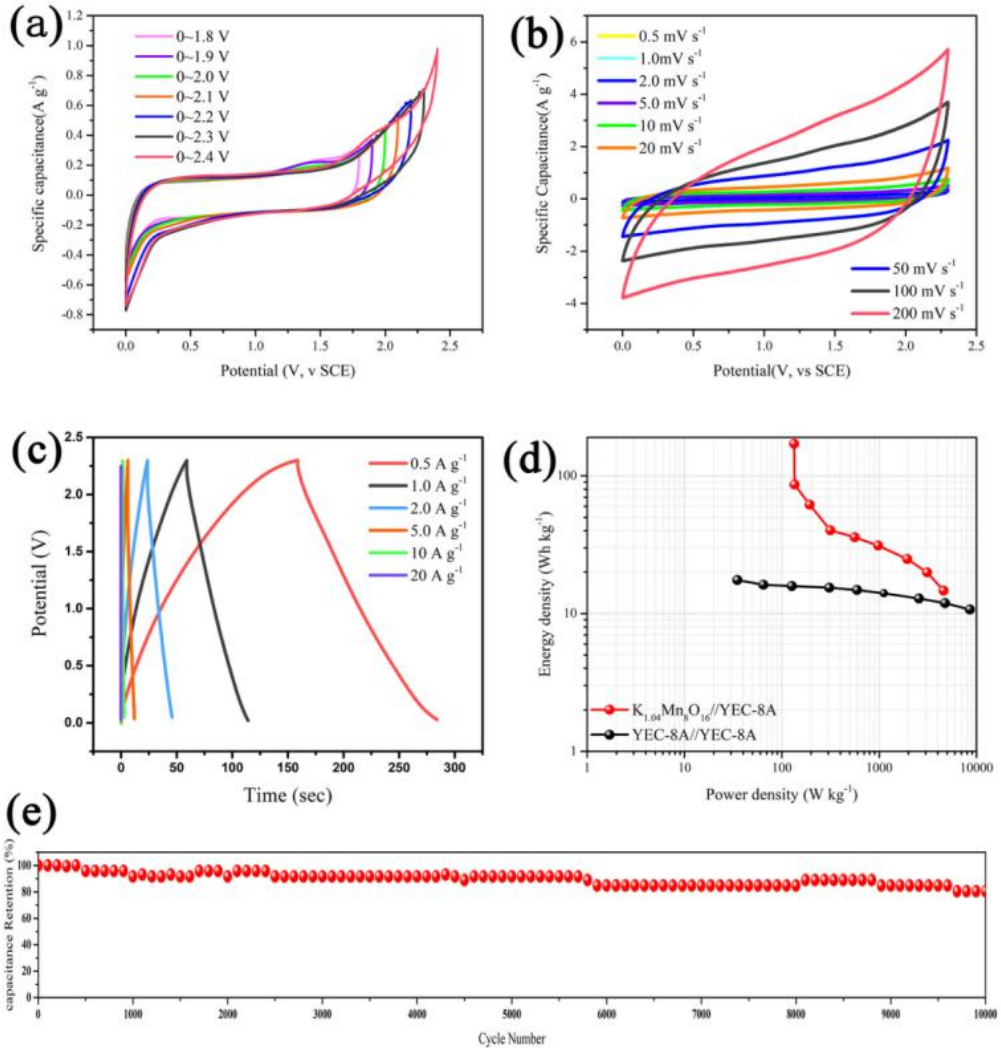

Fig. 7. Electrochemical performance of the KMO//YEC electrodes in Na-ion hybrid capacitors:(a) CV curves under different voltage windows. (b) CV curves under different scan rates. (c) The typical charge-discharge profiles at various current densities. (d) Ragone plots . (e) Long cycle performance.

Electrochemical properties of YEC were tested in Na_2SO_4 aqueous electrolyte

and shown in Fig. S2. The CV curves are approximately rectangular at different scan rates ranging from 0.5 to 200 mV s^{-1}, and the curves of constant current charge and discharge are symmetrical straight lines. It shows excellent capacitance performance of up to 155.59 F g^{-1} at 0.5 mV s^{-1}. To assemble hybrid capacitors, the mass ratio of KMO cathode and YEC anode is calculated to be 1:2. The CV curves at different voltage windows of KMO//YEC hybrid device is shown in Fig. 7a. It can be seen that even when the voltage window increases to 2.4 V, the hybrid overcharge remains stable. The CV curves of KMO//YEC at different scan rates from 0.5 to 200 mV s^{-1} is shown in Fig. 7b. And the charge/discharge profiles at various densities from 0.5 to 20 A g^{-1} is shown in Fig. 7c, symmetrical curves show the storage reversibility of capacitors.

The Ragone plots of power densities and energy densities b is shown in Fig. 7d. It achieves a high energy density of 170.96 Wh kg^{-1} at the power density of 133.79 W kg^{-1}, and high power density of 3 kW kg^{-1} at the energy density of 19.88 Wh kg^{-1}. These are higher than activated carbon YEC symmetrical capacitor and some other reports and shown in Table 3. The cycle performance of KMO at a current density of 1 A g^{-1} is shown in Fig. 7e. The capacitance retains 85% over 10000 cycles.

Table 3. Comparison of power density and energy density of Na-ion hybrid supercapacitors(NIHS).

Hybrid	Technology	Energy (Wh kg^{-1})	Power (W kg^{-1})	Ref.
KMO//YEC	NIHS	170.96	133.79	This work in Na_2SO_4
AC//Na-TNT	NIHS	107.16	32.99	[40]

AC//V_2O_5/CNT	NIHS	39.77	135.62	[41]
GF//NTO/CT	NIHS	55	200	[42]

4. Conclusion

In summary, potassium-ion pre-inserted $K_xMn_8O_{16}$ materials consist of nanoparticles and nanorods were prepared by facile high-temperature calcination. This unique structure is good for achieving excellent electrochemical performance, since nanoparticles can greatly increase the internal area to make sure that the electrolyte is in full contact with the active material, and nanorods furnish short ion diffusion pathways during charging/discharging process. The Li-ion and Na=ion hybrid supercapacitors assembled with KMO and activated carbon exhibitoutstanding electrochemical behavior. Both of the hybrid devices show higher energy densities and power densities than symmetric capacitors and hybrid capacitros reported previously. The capacitance retention of Li-ion capacitor and Na-ion capacitor after 10000 cycles is 97% and 85%, respectively. Therefore, this kind of material embedded with potassium ion manganese nanostructure has excellent electrochemical properties and broad application prospects.

References:

1. Wei, W.; Cui, X.; Chen, W.; Ivey, D. G., Manganese oxide-based materials as electrochemical supercapacitor electrodes. *Chemical society reviews* **2011,** *40* (3), 1697-1721.

2. Guan, B. Y.; Kushima, A.; Yu, L.; Li, S.; Li, J.; Lou, X. W., Coordination Polymers Derived General Synthesis of Multishelled Mixed Metal-Oxide Particles for Hybrid Supercapacitors. *Advanced Materials* **2017,** *29* (17), 1605902.

3. Ding, J.; Hu, W.; Paek, E.; Mitlin, D., Review of Hybrid Ion Capacitors: From Aqueous to Lithium to Sodium. *Chemical Reviews* **2018,** *118* (14), 6457-6498.

4. Sharma, P.; Bhatti, T. S., A review on electrochemical double-layer capacitors. *Energy Conversion and Management* **2010,** *51* (12), 2901-2912.

5. Choi, N. S.; Chen, Z.; Freunberger, S. A.; Ji, X.; Sun, Y. K.; Amine, K.; Yushin, G.; Nazar, L. F.; Cho, J.; Bruce, P. G., Challenges facing lithium batteries and electrical double-layer capacitors. *Angewandte Chemie International Edition* **2012,** *51* (40), 9994-10024.

6. Wang, F.; Wu, X.; Yuan, X.; Liu, Z.; Zhang, Y.; Fu, L.; Zhu, Y.; Zhou, Q.; Wu, Y.; Huang, W., Latest advances in supercapacitors: from new electrode materials to novel device designs. *Chemical Society Reviews* **2017,** *46* (22), 6816-6854.

7. Wang, Y.; Shi, Z.; Huang, Y.; Ma, Y.; Wang, C.; Chen, M.; Chen, Y., Supercapacitor devices based on graphene materials. *The Journal of Physical Chemistry C* **2009,** *113* (30), 13103-13107.

8. Meng, Q.; Cai, K.; Chen, Y.; Chen, L., Research progress on conducting polymer

based supercapacitor electrode materials. *Nano Energy* **2017,** *36*, 268-285.

9. Wang, Y.-g.; Xia, Y.-y., A new concept hybrid electrochemical surpercapacitor: Carbon/$LiMn_2O_4$ aqueous system. *Electrochemistry Communications* **2005,** *7* (11), 1138-1142.

10. Kumar, N.; Guru Prasad, K.; Maiyalagan, T.; Sen, A., Precise control of morphology of ultrafine $LiMn_2O_4$ nanorods as a supercapacitor electrode via a two-step hydrothermal method. *CrystEngComm* **2018,** *20* (38), 5707-5717.

11. Wang, F.; Xiao, S.; Zhu, Y.; Chang, Z.; Hu, C.; Wu, Y.; Holze, R., Spinel LiMn2O4 nanohybrid as high capacitance positive electrode material for supercapacitors. *Journal of Power Sources* **2014,** *246*, 19-23.

12. Lv, Z.; Luo, Y.; Tang, Y.; Wei, J.; Zhu, Z.; Zhou, X.; Li, W.; Zeng, Y.; Zhang, W.; Zhang, Y., Editable supercapacitors with customizable stretchability based on mechanically strengthened ultralong MnO2 nanowire composite. *Advanced Materials* **2018,** *30* (2), 1704531.

13. Largeot, C.; Portet, C.; Chmiola, J.; Taberna, P.-L.; Gogotsi, Y.; Simon, P., Relation between the ion size and pore size for an electric double-layer capacitor. *Journal of the American Chemical Society* **2008,** *130* (9), 2730-2731.

14. Xu, W.; Jiang, Z.; Yang, Q.; Huo, W.; Javed, M. S.; Li, Y.; Huang, L.; Gu, X.; Hu, C., Approaching the lithium-manganese oxides' energy storage limit with Li2MnO3 nanorods for high-performance supercapacitor. *Nano Energy* **2018,** *43*, 168-176.

15. Lin, Y.-P.; Wu, N.-L., Characterization of $MnFe_2O_4/LiMn_2O_4$ aqueous asymmetric supercapacitor. *Journal of Power Sources* **2011,** *196* (2), 851-854.

16. Mu, C.; Lou, S.; Ali, R.; Xiong, H.; Liu, S.; Wang, H.; Huo, W.; Yin, L.; Jia, R.; Liu, Y.; Jian, X., Carbon-decorated $LiMn_2O_4$ nanorods with enhanced performance for supercapacitors. *Journal of Alloys and Compounds* **2019,** *805*, 624-630.

17. Karikalan, N.; Karuppiah, C.; Chen, S.-M.; Velmurugan, M.; Gnanaprakasam, P., Three-Dimensional Fibrous Network of $Na_{0.21}MnO_2$ for Aqueous Sodium-Ion Hybrid Supercapacitors. *Chemistry – A European Journal* **2017,** *23* (10), 2379-2386.

18. Guo, W.; Yu, C.; Li, S.; Wang, Z.; Yu, J.; Huang, H.; Qiu, J., Strategies and insights towards the intrinsic capacitive properties of MnO_2 for supercapacitors: Challenges and perspectives. *Nano Energy* **2018**.

19. Chen, S.; Zhu, J.; Wu, X.; Han, Q.; Wang, X., Graphene oxide−MnO_2 nanocomposites for supercapacitors. *ACS nano* **2010,** *4* (5), 2822-2830.

20. Cakici, M.; Kakarla, R. R.; Alonso-Marroquin, F., Advanced electrochemical energy storage supercapacitors based on the flexible carbon fiber fabric-coated with uniform coral-like MnO_2 structured electrodes. *Chemical Engineering Journal* **2017,** *309*, 151-158.

21. Du, W.; Wang, X.; Zhan, J.; Sun, X.; Kang, L.; Jiang, F.; Zhang, X.; Shao, Q.; Dong, M.; Liu, H., Biological cell template synthesis of nitrogen-doped porous hollow carbon spheres/MnO_2 composites for high-performance asymmetric supercapacitors. *Electrochimica Acta* **2019,** *296*, 907-915.

22. Wu, Z.-S.; Ren, W.; Wang, D.-W.; Li, F.; Liu, B.; Cheng, H.-M., High-energy MnO_2 nanowire/graphene and graphene asymmetric electrochemical capacitors. *ACS nano* **2010,** *4* (10), 5835-5842.

23. Yu, G.; Hu, L.; Liu, N.; Wang, H.; Vosgueritchian, M.; Yang, Y.; Cui, Y.; Bao, Z., Enhancing the supercapacitor performance of graphene/MnO_2 nanostructured electrodes by conductive wrapping. *Nano letters* **2011,** *11* (10), 4438-4442.

24. Toupin, M.; Brousse, T.; Bélanger, D., Charge Storage Mechanism of MnO_2 Electrode Used in Aqueous Electrochemical Capacitor. *Chemistry of Materials* **2004,** *16* (16), 3184-3190.

25. Dong, S.; Li, Z.; Xing, Z.; Wu, X.; Ji, X.; Zhang, X., Novel Potassium-Ion Hybrid Capacitor Based on an Anode of $K_2Ti_6O_{13}$ Microscaffolds. *ACS Applied Materials & Interfaces* **2018,** *10* (18), 15542-15547.

26. Abdollahifar, M.; Huang, S.-S.; Lin, Y.-H.; Sheu, H.-S.; Lee, J.-F.; Lu, M.-L.; Liao, Y.-F.; Wu, N.-L., Tetragonal $LiMn_2O_4$ as dual-functional pseudocapacitor-battery electrode in aqueous Li-ion electrolytes. *Journal of Power Sources* **2019,** *412*, 545-551.

27. Wang, F. X.; Xiao, S. Y.; Zhu, Y. S.; Chang, Z.; Hu, C. L.; Wu, Y. P.; Holze, R., Spinel $LiMn_2O_4$ nanohybrid as high capacitance positive electrode material for supercapacitors. *Journal of Power Sources* **2014,** *246*, 19-23.

28. Jiang, J.; Li, J.; Long, X.; Zhao, D.; Su, K.; Xv, D.; Yang, C.; Qian, D., Sol–gel synthesis of $K_{1.33}Mn_8O_{16}$ nanorods and their applications for aqueous K-ion hybrid supercapacitors. *Materials Research Bulletin* **2019,** *109*, 29-33.

29. Chen, L.; Chen, L.; Zhai, W.; Li, D.; Lin, Y.; Guo, S.; Feng, J.; Zhang, L.; Song, L.; Si, P.; Ci, L., Tunable synthesis of Li_xMnO_2 nanowires for aqueous Li-ion hybrid supercapacitor with high rate capability and ultra-long cycle life. *Journal of Power*

Sources **2019,** *413*, 302-309.

30. Li, S.; Wen, J.; Mo, X.; Long, H.; Wang, H.; Wang, J.; Fang, G., Three-dimensional MnO_2 nanowire/ZnO nanorod arrays hybrid nanostructure for high-performance and flexible supercapacitor electrode. *Journal of Power Sources* **2014,** *256*, 206-211.

31. Yu, F.; Chang, Z.; Yuan, X.; Wang, F.; Zhu, Y.; Fu, L.; Chen, Y.; Wang, H.; Wu, Y.; Li, W., Ultrathin $NiCo_2S_4$@ graphene with a core–shell structure as a high performance positive electrode for hybrid supercapacitors. *Journal of Materials Chemistry A* **2018,** *6* (14), 5856-5861.

32. Kim, E.; Kim, H.; Park, B. J.; Han, Y. H.; Park, J. H.; Cho, J.; Lee, S. S.; Son, J. G., Etching-Assisted Crumpled Graphene Wrapped Spiky Iron Oxide Particles for High-Performance Li-Ion Hybrid Supercapacitor. *Small* **2018,** *14* (16), 1704209.

33. Jiang, J.; Kucernak, A., Electrochemical supercapacitor material based on manganese oxide: preparation and characterization. *Electrochimica Acta* **2002,** *47* (15), 2381-2386.

34. Miyakoshi, A.; Ueno, A.; Ichikawa, M., XPS and TPD characterization of manganese-substituted iron–potassium oxide catalysts which are selective for dehydrogenation of ethylbenzene into styrene. *Applied Catalysis A: General* **2001,** *219* (1), 249-258.

35. Lv, X.; Zhang, H.; Wang, F.; Hu, Z.; Zhang, Y.; Zhang, L.; Xie, R.; Ji, J., Controllable synthesis of MnO_2 nanostructures anchored on graphite foam with different morphologies for a high-performance asymmetric supercapacitor.

CrystEngComm **2018,** *20* (12), 1690-1697.

36. Liu, C.-l.; Luo, S.-h.; Huang, H.-b.; Zhai, Y.-c.; Wang, Z.-w., Layered potassium-deficient P2-and P3-type cathode materials K_xMnO_2 for K-ion batteries. *Chemical Engineering Journal* **2019,** *356*, 53-59.

37. Kim, H.; Park, K. Y.; Cho, M. Y.; Kim, M. H.; Hong, J.; Jung, S. K.; Roh, K. C.; Kang, K., High-Performance Hybrid Supercapacitor Based on Graphene-Wrapped $Li_4Ti_5O_{12}$ and Activated Carbon. *ChemElectroChem* **2014,** *1* (1), 125-130.

38. Feng, J.; Chernova, N. A.; Omenya, F.; Tong, L.; Rastogi, A. C.; Whittingham, M. S., Effect of electrode charge balance on the energy storage performance of hybrid supercapacitor cells based on $LiFePO_4$ as Li-ion battery electrode and activated carbon. *Journal of Solid State Electrochemistry* **2018,** *22* (4), 1063-1078.

39. Gao, H.; Wang, J.; Zhang, R.; Wu, L.; Tao, C.-a.; Deng, G., An aqueous hybrid lithium ion capacitor based on activated graphene and modified LiFePO4 with high specific capacitance. *Materials Research Express* **2019,** *6* (4).

40. Yin, J.; Qi, L.; Wang, H., Sodium titanate nanotubes as negative electrode materials for sodium-ion capacitors. *ACS applied materials & interfaces* **2012,** *4* (5), 2762-2768.

41. Chen, Z.; Augustyn, V.; Jia, X.; Xiao, Q.; Dunn, B.; Lu, Y., High-performance sodium-ion pseudocapacitors based on hierarchically porous nanowire composites. *ACS nano* **2012,** *6* (5), 4319-4327.

42. Dong, S.; Shen, L.; Li, H.; Pang, G.; Dou, H.; Zhang, X., Flexible sodium-ion pseudocapacitors based on 3D $Na_2Ti_3O_7$ nanosheet arrays/carbon textiles anodes.

Advanced Functional Materials **2016,** *26* (21), 3703-3710.